An operational workflow to assess rice nutritional status based on satellite remote sensing and smart apps

Francesco Nutini[a,*], Roberto Confalonieri[b], Alberto Crema[a], Ermes Movedi[b], Livia Paleari[b], Dimitris Stavrakoudis[c], Mirco Boschetti[a,*]

[a] IREA, National Research Council, Via Bassini 15, 20133 Milano, Italy

[b] Cassandra Lab, DESP, Università degli Studi di Milano, Via Celoria 2, 20133 Milan, Italy

[c] Laboratory of Forest Management and Remote Sensing, School of Forestry and Natural Environment, Aristotle University of Thessaloniki, Thessaloniki 54124, Greece

* Corresponding authors.

E-mail addresses: nutini.f@irea.cnr.it (F. Nutini), boschetti.m@irea.cnr.it (M. Boschetti).

Abstract

Nitrogen fertilization plays a key role in rice productivity and environmental impact of rice-based cropping systems, as well as on farmers' income, representing one of the main cost items of rice farming. Average nitrogen use efficiency in rice paddies is often very low (about 30%), leading to groundwater contamination, greenhouse gases emission, and economic losses for farmers. The resulting pressure on many actors in the rice production chain has generated a need for operational tools and techniques able to increase nitrogen use efficiency. We present an operational workflow for producing nitrogen nutritional index (NNI) maps at sub-field scale based on the combined use of high-resolution satellite images and ground-based estimates of Leaf Area Index (LAI) and plant nitrogen concentration (PNC, %) data collected using smart apps. The workflow was tested in northern Italy. The analysis reveals that vegetation indices are satisfactorily correlated with LAI ($r2 > 0.77$, $p < 0.01$) and PNC ($r2 > 0.55$, $p < 0.01$); whereas most patterns of NNI maps are coherent with the available information on soil texture and performed agro-practices. Key features of the proposed approach are (i) the time and cost-effectiveness for producing NNI maps even in operational contexts and (ii) the full exploitation of smart scouting techniques to drive field data acquisitions using smartphones as sensors. The use of operational, free-of charge products from Sentinel-2 for real-time field monitoring to potentially support variable rate fertilizations is also discussed.

1. Introduction

Nitrogen (N) is a key element for plant growth, being a fundamental component of many cell structures such as proteins, chlorophylls and nucleic acids. Its concentration in plant tissues is the highest among those of the three main nutritional elements for plants (N, phosphorus [P] and potassium [K]). For instance, Sukristiyonubowo et al. (2012) measured N, P and K contents in rice (Oryza sativa L.) grains corresponding to 1.28%, 0.15% and 0.32% on dry matter basis, respectively. For these reasons, rice N demand is high and deficiencies rapidly decrease yields (Huang et al., 2015), because of reduced tillering, lower number of spikelets per panicle and decreased photosynthetic rate (Mae, 1997). However, rice yields are also threatened by N excess, because of the increased plant susceptibility to diseases (Long et al., 2000) and lodging (Shimono et al., 2007). The high impact of N availability on yields and the low efficiency in its use due to the special water management practices applied to rice paddies, make it crucial for paddy rice farmers to match plants needs with supply in terms of both timing and amounts. Concerning the low N use efficiency, most of the N supplied to paddies can be lost via denitrification because of the redox conditions of flooded soils, ammonia volatilization, and—especially in case of dry sowing and delayed flooding on non-puddled soils—nitrate leaching (Confalonieri et al., 2006; Ke et al., 2017). According to published data, N use efficiency in rice paddies range from about 60% at best (Li et al., 2017) to 12% in the worst cases (Singh et al., 1999), with common values reported to be around 30% (e.g., Confalonieri et al., 2006). These low efficiencies lead to eutrophication, groundwater contamination, greenhouse gases emission and air pollution. In order to mitigate these impacts and to avoid excessive fertilization, the EC Nitrate Directive (91/676/EEC) focuses on encouraging a stricter and mindful application of nitrogen. Another crucial factor relevant to the low N use efficiencies often observed in paddy fields is related to the impact on farmers' income, since fertilization is a major cost in rice farming. For example, in Italy, a major rice producer in Europe, the cost for fertilizers in a medium-size rice farm (150 ha) represents almost 40% (~370 €/ha) of the total cost for input factors, with agrochemicals, seeds and water accounting only for 26%, 16%, and 20%, respectively (Camera di Commercio Vercelli, 2013). This further underlines how fertilizers management is of fundamental importance for farm economic balance. In this context, operational solutions able to optimize the use of N fertilizers are increasingly needed to implement sustainable agro-practices and maximize farmers' income, in other words, to increase the efficiency of rice-based cropping systems. A promising approach to face this challenge is precision farming, i.e., the exploitation of multi-source information in a decision support system to improve the efficiency of farm management (Blackmore, 1994).

1.1. Precision farming and variable rate technologies for fertilization

The use of variable rate (VR) fertilization maps rather than fertilizing homogeneously the whole field is considered a promising approach to face some of the criticalities involved with N use efficiency and represents the basis for the implementation of rationale top-dressing fertilization (Basso et al., 2016). Indeed, the capacity to assess, understand and manage the within-field variability is a prerequisite to define sustainable agro-practices able to reduce farming cost and environmental impact (Stroppiana et al., 2009). Different methodologies were proposed in recent years, some of them being operationally adopted in real farming practices to create variability maps. These methodologies can be grouped in two categories: (i) based on the analysis of static information from data acquired during previous cropping season(s) and (ii) based on the near-real-time dynamic monitoring of crop conditions exploiting direct/indirect measurements. A common approach for supporting the creation of VR maps is to exploit different thematic layers as input to a clustering process, in order to generate a map of management unit zones (MUZ) where each zone represents an area with uniform condition of soil fertility to be appropriately managed (Fridgen et al., 2004). Spatially-distributed inputs for MUZ definition can refer to every kind of information related to plant growth and considered important for yield determination (Casa and Morari, 2016). For instance, MUZ can be identified through the analysis of soil properties either derived from (i) interpolation of geolocated ground data of "stable" soil parameters, like texture, organic matter content, available phosphorus, and exchangeable potassium (Casa and Castrignanò, 2008; Casa and Morari, 2016) and/or (ii) indirectly estimated from the analysis of remote sensing data (e.g., Agbu et al., 1990) or ground measurements (e.g., soil electrical conductivity; Grisso et al., 2009). Alternatively, yield maps produced in previous years (Stafford et al., 1999) or archives of remote sensing (RS) data can also be used to define patterns of constant intra-field variability (Busetto et al., 2017; Casa et al., 2017). The definition of MUZ can be continuously updated to account for new information made available by new technologies (e.g., new satellites, drones, new sensors) or by more recent yield maps. Another approach for static VR fertilization is based on compiling a simplified nutrient balance (Grignani et al., 2003). This can be performed by analyzing yield maps from previous seasons to get spatially distributed estimates of the uptake of main nutrients (N, P, K), as well as inferring the other items of the balance, such as residuals from previous organic fertilizations, inputs from dry and wet depositions, losses from leaching and so on (Casa et al., 2011). The fertilization for the current season can be then modulated based on the expected crop needs (Casa et al., 2011). Compared to the approaches previously described, for which fertilizer amounts can be quantified only via expert knowledge, the nutrient balance approach allows mapping explicitly the quantity of fertilizers, although it requires more inputs. Dynamic monitoring for VR fertilization is instead based on the near-real-time collection of data able to provide information on crop development and nutrition status. For this approach, ground, proximal and remote sensing measurements are usually exploited to analyze the within-field variability in a qualitative or quantitative way. One of the main constraints in using optical sensors to map nutritional status is the fact that N content is not an optically discernible variable in green plants, because nitrogen absorption features are obscured by water (Chen, 2015). Therefore, it cannot be estimated directly from RS. However, it is possible to assess N concentration thanks to its direct relationship with chlorophyll content that has well-known spectral features in visible and Red-Edge bands. For this reason, chlorophyll related indicators can be used as proxies of crop nitrogen concentration (Guerif et al., 2007). A qualitative approach to support in-season VR fertilization can rely on the analysis of spatially distributed information (from the interpolation of field measurements or from proximal/remote sensing images) in order to identify field regions characterized by different crop vigor. In this sense, recent approaches are driven by sensors mounted directly on the operating tractor (e.g., GreenSeeker active canopy sensor; Trimble, Sunnyvale, CA, USA), or by the analysis of earth observation (EO) data acquired by sensors on drones, aircraft or satellites (Casa and Morari, 2016). According to the within-field variability in crop vigor, N application can be modulated either (i) using cultivar specific empirical equations (Xue and Yang, 2008; Pahlmann et al., 2017) or (ii) adapting the average prescription (based on expert knowledge) in the different zones according to the relationship between local crop vigor and field average (Busetto et al., 2017). These approaches are already provided by operational services exploiting commercial devices such as those proposed by Oklahoma State University for GreenSeeker (Raun et al., 2005) or by Nebraska University for Crop Circle (Holland and Schepers, 2010). Other approaches for dynamic VR fertilization are more quantitative and provide a direct support to farmer by diagnosing the actual crop N nutritional status. A widely recognized approach is the one based on the estimation of N nutritional index (NNI) (Lemaire et al., 2008). NNI is the ratio between actual (PNC, %) and critical (Nc, %) plant N concentration, with the latter being the minimum N concentration below which crop growth is reduced and the former is the plant nitrogen concentration (Confalonieri et al., 2011). Nc is often estimated as a function of aboveground biomass (AGB) using the dilution curve approach (Salette and Lemaire, 1981; Ata-Ul-Karim et al., 2013), with its value decreasing during the crop cycle because of the reallocation of N-rich compounds from senescent tissues and of the relative decrease in N-rich organs during crop aging (less leaves, more stems) (Confalonieri et al., 2011). Other approaches derive Nc curves as a function of development stage indices (Williams et al., 1989; Hansen et al., 1991). In any case, the effectiveness of these methods for diagnostic purposes is partly limited by the procedures needed to determine their driving variables (AGB or development stage indices). To overcome this limitation, a recent approach was proposed to derive Nc curves as a function of Leaf Area Index (LAI) (Confalonieri et al., 2011), easily obtainable using indirect, non-destructive methods (e.g., LAI-2000; (Stroppiana et al., 2006)) without the need for defining sample size, sampling/drying/weighing plants (as for AGB determination), or performing calculations based on heat units (as for development stage indices). As for LAI, instruments are available for non-destructive PNC estimates (through related index and dedicated calibration curves (Varinderpal et al., 2011)). Examples range from inexpensive plastic strips with different green shades (leaf color charts; (Alam et al., 2005)) to optical instruments able to estimate plant chlorophyll content alone (e.g., SPAD 502, Konica Minolta Inc., Tokyo, Japan; (Peng et al., 1996)) or in addition to other variables related to the relationship between primary and secondary metabolism (flavonoids content) to derive a N balance index (Dualex 4, Force-A, Orsay, France; (Cerovic et al., 2012)). Other approaches were proposed based on the exploitation of hyperspectral proximal sensing measurements (Stroppiana et al., 2009). Recently, new approaches were proposed to estimate both LAI (Confalonieri et al., 2013) and PNC (Confalonieri et al., 2015) using sensors available on smartphones. These approaches—implemented through two dedicated Android smart apps (i.e., PocketLAI and PocketN)—represent indeed a promising source of quick, inexpensive, and accurate ground data for monitoring N nutritional status, increasing the feasibility of in-field crop status assessment. The use of field data and the Nc curve for near-real-time assessment of N nutritional status can be boosted by exploiting satellite images from space-mounted sensors (Munoz-Huerta et al., 2013), since they incorporate spectral bands useful for the retrieval and estimation of LAI and chlorophyll content (Navarro-Cerrillo et al., 2014). Approaches based on EO data can overcome the limitations imposed by field data collection, such as the high cost involved and representativeness of the data collected. Indeed, NNI estimated in field can be directly spatialized using RS images via empirical relationships between NNI and a simple vegetation index (VI) (Cao et al., 2013) or complex VI combinations (Fitzgerald et al., 2010). Alternatively, it is possible to indirectly estimate NNI (Huang et al., 2015) using PNC and Nc values—the latter derived either using AGB (Chen et al., 2010; Cilia et al., 2014) or LAI (Ata-Ul-Karim et al., 2014)—at pixel level from satellite data and relationships with VIs, and then use spatially-distributed PNC and Nc values to derive NNI. These two approaches have been compared by Huang et al. (2015) and Chen (2015), resulting in a slightly better accuracy of NNI estimation with indirect approach. This approach is in fact operatively exploited by the Farmstar service to produce prescription maps for winter cereals (Triticum aestivum L., Hordeum vulgare L.), soybean (Glycine max L. Merr.), and rapeseed (Brassica napus L.) in France (Blondlot et al., 2005). The general goal of this study was to setup and test an operational workflow able to spatialize indirect field estimates of LAI and PNC using satellite data to retrieve NNI maps for rice. In particular, the study aims to (i) demonstrate the efficiency of EO-based smart scouting to optimize and drive field measurements, (ii) exploit smart apps to collect relevant field data (LAI, PNC), and (iii) test the potential of commercial and Sentinel-2 data for NNI estimates in operational precision farming contexts.

2. Materials and methods

2.1 Study area

The study was carried out in 2016 in an area sited in the middle of the main Italian rice district, in turn located in the Northern part of the Country and covering about 240000 ha of paddies producing about 90% of Italian rice (almost 50% of total European production; Fig. 1). In this area, rice is sown between April and May and harvested between September and October, depending on rice varieties, weed control (false sowing), and seasonality (Boschetti et al., 2017, 2009; Busetto et al., 2017). About half of the district is sown with long-grain Japonica varieties for internal consumption, with the remaining part destined to long-grain Tropical Japonica (26%) and short-grain Japonica varieties (23%) that are mainly exported in EU-27 (NOMISMA, 2013). Agriculture is highly mechanized and usually rice is grown in monoculture, not being part of rotations with other species.

The amount of N yearly supplied to rice paddies is 150 kg ha^{-1}, usually split in two (pre-sowing and panicle initiation (BBCH 31)) or three events (an additional event at the beginning of tillering (BBCH21)). How the total amount of nitrogen is split between the three events and the type of fertilized used vary a lot according to farmers' experience, variety, and agronomical planning.

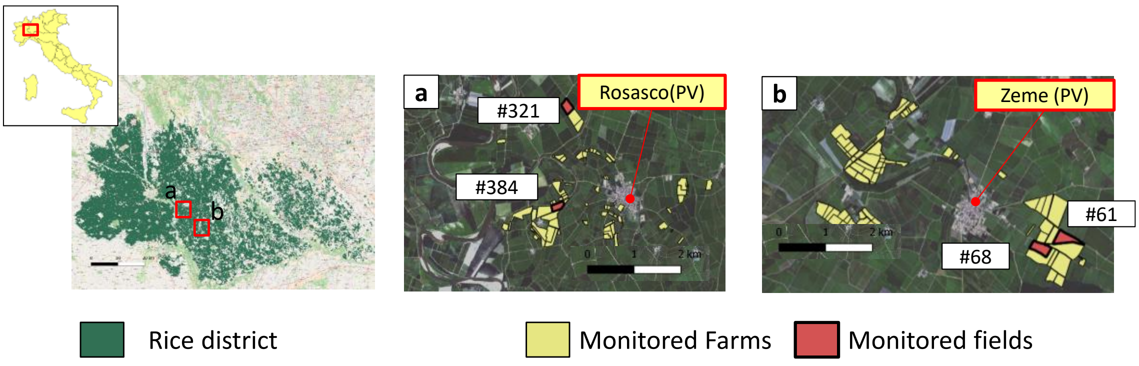

Figure 1. Italian rice district (green areas in left panel) and location of the monitored fields in Rosasco (a) and Zeme (b) municipalities. Numbers refer to field IDs. A RapidEye image in true colors is used as background.

The fields of interest (FOI; red polygons in Fig. 1) are located in Pavia province (PV), where rice covers 70% of the agricultural surface, other common crops being soybean and corn. The monitored fields belong to two farmers involved in the ERMES project (an Earth obseRvation Model based ricE information Service, www.ermes-fp7space.eu) as end-users. The project aimed at developing downstream services dedicated to the rice sector to support authorities and farmers (Busetto et al., 2017). The monitored fields (about 20 ha) were sown in May with Selenio (a short-grain Japonica variety quite popular in Italy). Two different sowing techniques were used: scatter-sowing under flooded conditions and row-sowing with delayed flooding at the fifth-leaf stage (Campos-Taberner et al., 2016; Ranghetti et al., 2016) (Table 1).

Table 1. Monitored fields.

Field Id	Extension [ha]	Municipality	Coordinates [Lon. E, Lat. N]	Sowing day of the year	Sowing technique
#1	4.4	Rosasco	8.564, 45.266	127	Row/dry
#2	3.2	Rosasco	8.561, 45.248	145	Row/dry
#3	5.9	Zeme	8.682, 45.191	138	Row/dry
#4	6.8	Zeme	8.688, 45.192	138	Scatter/flooded

2.2 Overall methodolody

The experimental activity was articulated in three main steps (Figure 2): *i)* acquisition of field data according to a smart scouting procedure, *ii)* satellite data processing and correlation analysis with crop biophysical variables and *iii)* map generation and assessment of NNI.

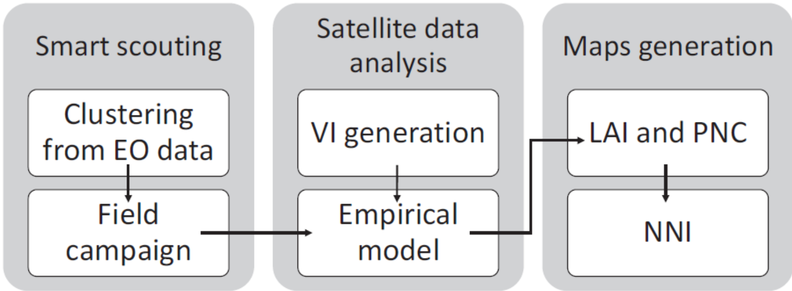

Figure 2: Flowchart of the methodology adopted. From left to right: Satellite-aid smart scouting activities to collect few representative field data (leaf area index [LAI] and plant nitrogen content [PNC]), analysis of satellite data for empirical model development and computation of nitrogen nutritional index (NNI) maps.

Satellite imagery acquired by the RapidEye sensor were used in all the three steps, i.e., from driving the field campaign (smart scouting) to the production of maps of biophysical variables via regression models, whereas Sentinel-2 data were tested only for the last two steps (empirical model and maps development). Details on data acquisition and on the three methodological steps are provided in the following sections.

2.3 Scheduling of activities, smart scouting and field measurements

Farmers participating to the study provided information on field boundaries, soil analyses, sown varieties, and crop management (Table 2). This information was used *i)* to identified four fields with similar size (larger than 3 ha) and sowing date (time-span of maximum 20 days), and where the same variety was grown (Selenio), as well as *ii)* to plan field measurements and satellite image acquisition. Farmers' knowledge was also fundamental to discuss results and NNI spatial patterns identified for the different fields.

Table 2. Timetable of satellite image acquisitions and relationships with relevant management events in the four monitored fields.

Date	7th-25t^{h} May	18th-22nd June	1st July	4th July	5th July	10th-14th July
Event	Sowing	1st top dressing fertilization	Sentinel-2 acquisition	RapidEye acquisition	Smart Scouting and field campaign	2nd top dressing fertilization

2.3.1 Selection and acquisition of satellinte images

RapidEye (RE) and Sentinel-2A (S2; free-of-charge) satellite image acquisitions were programmed and performed at the first week of July in order to match the phenological phase of panicle initiation (BBCH 31). This stage is of key importance for top-dressing fertilization given its marked effect on final yield (Onoyama et al., 2010).

The RE image exploited in this study was made available in the framework of the ERMES project thanks to the ESA-Copernicus Data Ware House program (DWH), which provides EO data for European Copernicus research projects (Jutz and Milagro-Pérez, 2017). The image was acquired on 4 July over an extent of 330 km^2 (about 15 km × 22 km) and covered the whole study area. Thanks to the 5 m spatial resolution and five multispectral bands with both Red-Edge (690-730 nm) and NIR (760-850 nm) bands, this sensor is well-suited for crop monitoring purpose (Kuenzer and Knauer, 2013). The RE image was delivered as orthorectified tiles in GeoTIFF format (in WGS84/UTM32N projection), with radiometric, geometric, and terrain corrections having been applied (Level 3A). The image was subsequently atmospherically corrected and converted into ground reflectance values, by means of the ATCOR algorithm (Richter and Schlaepfer, 2016).

The S2 image has a lower spatial resolution (no band higher than 10×10 m) than RE but it is operationally available free-of-charge every 10 days (from 2017 every 5 days thanks to the second satellite S2B), whereas RE images are acquired from a five satellites constellation (revisit time nominally daily off-nadir and 5.5 days at nadir) on demand only subject to payment of a fee. The S2 cloud-free image closest to the RE overpass was the one acquired on July 1, 2016 on tile 32TMR (orbit R065). A Level 1C product (top-of-atmosphere reflectance values in cartographic geometry) was downloaded via the Sentinel Open Hub (scihub.copernicus.eu) and top of canopy reflectance values were obtained after atmospheric correction using the sen2cor (Sentinel-2 atmospheric Correction) algorithm incorporated within the Sentinel-2 Toolbox. More details on S2 processing can be found in Campos-Taberner et al. (2017).

2.3.2 *Fast processing of satellite data and Smart Scouting*

RE image was processed right after the acquisition in order to calculate a proxy of vegetation vigor and biomass to highlight within field spatial patterns exploiting automatic processing chain developed during the ERMES project (Busetto et al., 2017). The workflow includes three consecutive steps to calculate: *i)* vegetation index map (VI), *ii)* relative variability map (Δ) and thematic maps (clusters).

The Modified soil-adjusted vegetation index (MSAVI) is calculated from the RE reflectance bands. The index was selected as the more useful in identifying biomass after literature review and thanks to previous test conducted in the framework of ERMES project exploiting 2014 and 2015 data. MSAVI map provides an absolute measure of the parcel's current status, that is dependent on sowing day, rice variety sowed, and so on. In order to transform this information into a relative measure (Δ), for each field of interest (FOI) the deviation of every image pixel (x) from the parcel's average (m) was calculated, through:

$$\mathrm{D(x) = x - m/m} \quad (1)$$

A relative variability map (Δ) that confines the values within the range [−1,1] is subsequently calculated, by applying a hyperbolic tangent (tanh) function:

$$\Delta(\mathrm{x}) = \mathrm{tanh}D(x) = \mathrm{tanh}(x - m/m) \quad (2)$$

This process was necessary in order to normalize *D* values in a closed range and reduce the influence of extreme outlier values that can significantly affect the identification of significant field variability. The last step of processing chain produces a thematic map, by assigning each FOI's pixel to one out of three possible categories: a) above (parcel's) average biomass/vigour (cluster-a), b) average biomass/vigour (cluster-b) and c) below average biomass/vigour (clustrer-c). The process was applied independently in each FOI (Figure 3). The Δ intra-parcel variability values are first clustered using the fuzzy C-means (FCM) clustering algorithm (Bezdek et al. 1984). FCM clusters the data based on their distance from their closest centre (prototype), which is placed by its learning algorithm near locations with high density points (i.e., the modes of the distribution). A statistical procedure is employed to determine whether one (homogeneous field), two or three clusters will be produced, which are then appropriately assigned to one of the three categories. It is the latter discretized version of the variability map that is most appropriate for applying VR fertilization with most of the available commercial machinery.

A complete description of the methodology will be the subject of a dedicated future publication.

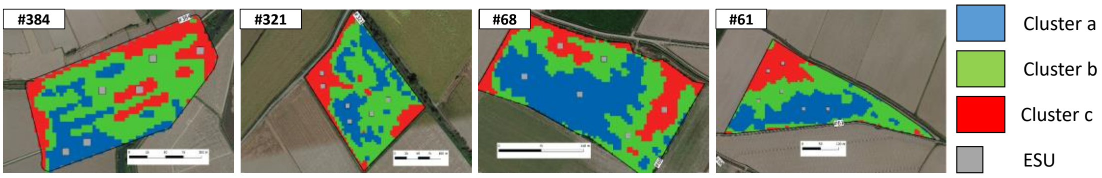

Figure 3. Clusters obtained from MSAVI map on the four analysed fields. Dark squares indicate the ESU, where measurements were conducted. For context, a RapidEye image in true colors is displayed in the background.

According to the generated cluster maps two location were identified in each cluster class and for each field producing a total of 24 (6 fields x 3 classes x 2 location) elementary sampling units (ESU). The ESUs were placed, if possible, away from field borders (at least two RE pixels from borders, i.e. 10 meters) and around the central part of MSAVI cluster. This approach is the base to conduct a "smart scouting" to collect field data, since it allowed us to place the ESUs in areas of greatest variability of rice biomass and status, avoiding time consuming and laborious random samplings.

Field campaigns were conducted two days after RE acquisition; data were acquired in correspondence of the identified ESUs thanks to a GPS rover unit (Trimble GEII Explorer) and following the sampling scheme described in the following section.

2.3.3 *Smart app measurements and field data collection*

The estimation of biophysical variables from satellite products via empirical modelling requires RS data to be compared with ground measurements for the corresponding variables. A bottom up approach is typically used for the validation/calibration strategy following international recognised protocol and guidelines as proposed by the CEOS LPV group (Morisette et al., 2006), the VALERI project (http://w3.avignon.inra.fr/valeri/), and ESA campaigns (Baret and Fernandes, 2012). The approach starts from the scale of the individual measurements that are aggregated over an Elementary Sampling Unit (ESU) with a support area consistent with that of the decametric product to be validated/calibrated (10-30 m). Several ESUs are sampled over a site, typically following a stratified sampling strategy (Cohen & Justice, 1999). This allows developing calibrated transfer functions between the radiometric signal, or bands combination, of a decametric sensor and crop variables.

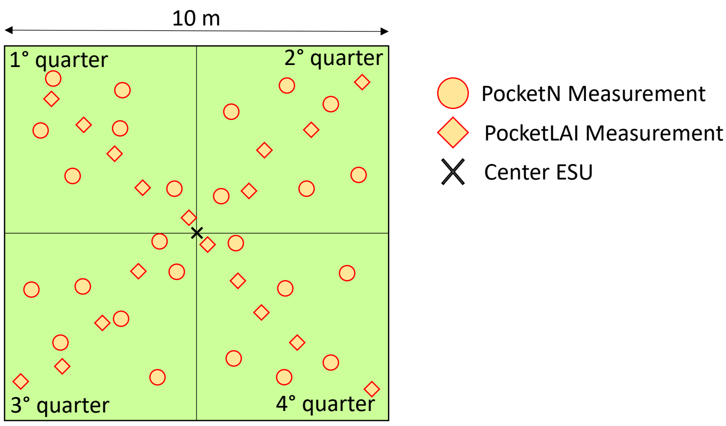

Figure 4: Sampling schemes of PocketN (#25 dots) and PocketLAI (#18 diamonds) data for an ESU.

For each ESU, 25 and 18 measurements were taken with the smart apps PocketN and PocketLAI, respectively (Figure 4). PocketLAI (Confalonieri et al., 2013) is based on the automatic segmentation of images acquired at 57.5° below the canopy while the used is rotating the device along its main axes, thanks to an inclinometer derived from the device accelerometer. At that zenith angle, the estimated gap fraction can be used to derive LAI using a light transmittance model that do not need either multi-angle measurements (like for LAI-2000) or parameters describing canopy structure (like for ceptometers) (Baret et al., 2010). PocketN (Confalonieri et al., 2015) is based on the estimation of the dark green colour index (DGCI, 0 to 1) according to Karcher and Richardson (2003) from leaf images acquired using a dedicated background panel that returns a flat reflectance across the visible spectrum to the device exposure meter, regardless of the illumination conditions during image acquisition. This allows normalizing the analysis of green shades during image processing. DGCI values from PocketN were converted into PNC values [mg/g]) using a calibration curve specifically developed for cv. Selenio (Confalonieri et al., 2015):

$$\mathrm{PNC} = (DGCI - \mathrm{a})/\mathrm{b} \tag{3}$$

with a and b being 0.3475 and 0.0776, respectively.

PocketLAI and PocketN demonstrated a comparable accuracy compared with commercial instruments, despite the advantages related with their cost and with the high portability (Confalonieri et al., 2013;2015). Further details on the functioning of both the apps are available in the seminal literature and, for PocketLAI, in the video tutorial at https://www.youtube.com/watch?v=qQPfzAxsGSs&t=13s. For each measuring point (Fig. 4), one PocketLAI estimate was taken below the canopy, and one PocketN reading was performed in the second third of the last completely emitted leaf blade of a random selected plant.

The dataset (432 and 600 values for PocketLAI and PocketN, respectively) was screened to detect errors or anomalous values, and then mean LAI and PNC values were calculated for each of the 24 ESU. When DGCI values were outside (lower) the range used to derive Eq. 3, they were set to the minimum values observed in the experimental condition.

2.4 Vegetation indices and correlation analsysis

RE and S2 images were used to calculate more than 20 VIs proposed for LAI and PNC estimates. Table 3 reports the indices considered, grouped according to the wavelengths they use. Details on indices formulation, original references, and sensors from which they can be calculated can be found in Index DataBase (indexdatabase.de, last access September 2017), whereas a short summary of this information is provided in Appendix. Indices based on bands in the shortwave infrared (SWIR) and Red-Edge(REdg) regions were calculated only for the S2 image. VI values were extracted from the pixels corresponding to each sampled ESUs and average values for each ESU were then computed. A buffer of 2×2 pixels from the ESU centroid for both RE (10m×10 m) and S2 (20m×20 m) images was considered while extracting VI data. After the elimination of two ESUs characterized by anomalous reflectance or PocketN data values, a total of 22 records were used to derive the relationships between field data (PNC and LAI) and VIs (from RE and S2 images). The best indices were selected based on the values of adjusted r^2 obtained from the regression analysis. The four linear models selected (two biophysical variables for each one of the two sensors) were then used to produce the respective LAI and PNC maps.

Table 3. VI used in the study as computed from RE and/or S2 images. VI are grouped on the basis of the wavelengths used. Vis=visible ([400–700 nm]; RE bands: 1,2,3; S2 bands: 2,3,4); REdg=red edge ([700–750 nm]; RE band: 4; S2 bands: 5,6,7); NIR=near infrared ([800–900 nm]; RE band: 5; S2 band: 8); SWIR: Short wave infrared ([1500–2500 nm]; S2 bands: 12, 13); Multiple Vis Ratio=VIs ratio.

Category*	Formula type	Index	Sensor
Vis	Normalized difference	GLI	Both
	Single band	Blue	Both
	Single band	Green	Both
	Single band	Red	Both
Vis-REdg	Simple ratio	PSSR	S2 only
	Addition/ subtraction	MCARI	Both
	Addition/ subtraction	TCARI	Both
	Normalized difference	NDVI2	S2 only
	Normalized difference	NDI45	S2 only
	Normalized difference	MTCI	S2 only
	Normalized difference	S2REP	S2 only
	Normalized difference	IRECI	S2 only
	Triangular	TCI	Both
Vis-REdg-NIR	Multiple ratio	DCNI	Both
Vis-REdg-SWIR	Addition/ subtraction	MCARI$_{SWIR}$	S2 only
	Addition/ subtraction	TCARI$_{SWIR}$	S2 only
Vis-NIR	Simple ratio	SR	Both
	Simple ratio	CI-G	Both
	Simple ratio	CVI	Both
	Addition/ subtraction	MSAVI	Both
	Normalized difference	NDVI	Both
	Normalized difference	SAVI	Both
	Normalized difference	EVI	Both
	Normalized difference	gNDVI	Both
	Normalized difference	OSAVI	Both
	Other	MTVI2	Both
Vis-SWIR	Normalized difference	NRI	S2 only
	Normalized difference	NDFI	S2 only
NIR-SWIR	Normalized difference	OSAVI$_{SWIR}$	S2 only
REdg-NIR	Simple ratio	CI-RE	Both
	Normalized difference	NDRE	Both
REdg	Single band	REd	Both
NIR	Single band	NIR	Both
Multiple Vis Ratio	VIs Ratio	MCARI/MTVI2	Both
	VIs Ratio	NDRE/NDVI	Both
	VIs Ratio	TCARI/SAVI	Both
	VIs Ratio	TCARI/OSAVI	Both
	VIs Ratio	TCARI/MSAVI	Both
	VIs Ratio	TCARI/OSAVI$_{SWIR}$	S2 only

2.5 Map generation and NNI estimation

After LAI and PNC layers were generated, Nc values – needed to calculate NNI – were derived from LAI data using Eq. 4:

$$\mathrm{PNC} = \frac{Nmat}{1 - e^{-k \cdot LAI}} \quad (4)$$

with k (0.5 in this study) and *Nmat* (1%) being the extinction coefficient for solar radiation and Nc at maturity, respectively (Confalonieri et al., 2011).

NNI maps derived from RE and S2 images were then compared to quantify the coherence of the two sensors and to evaluate the suitability of Sentinel-2 for assessing N nutritional status under operational conditions. Finally, NNI values extracted and averaged for each ESU were validated by comparing them with the NNI values directly calculated from field smart apps measurements.

3 Results and discussion

3.1 Analysis of smart app data

Boxplots of the field data collected with PocketLAI and PocketN over the ESUs are shown in Fig. 5a and b. Boxes' colors indicate the cluster from which the data were acquired (following the same color scheme with that of Fig. 3). LAI data ranged between 2.13 and 5.14, indirectly demonstrating the wide range of growing conditions explored thanks to the smart scouting. Data are coherent with the expected LAI values for rice at panicle initiation (Stroppiana et al., 2006; Xue and Yang, 2008; Huang et al., 2015). In particular, LAI from ESUs belonging to Cluster-a (blue) and Cluster-c (red) was the highest and the lowest respectively (Fig. 5a), which is coherent with the purpose of the clustering procedure and the semantics of the identified ESU classes. The same was observed for PNC (Fig. 5b), suggesting that the clustering procedure allowed identifying field points with different plant size and nutritional status. Compared to other studies carried out on real farming condition (e.g., Huang et al., 2015; Wang et al., 2017), field estimates were performed on a markedly lower number of points; still, the obtained range of LAI and PNC values is comparable. Indeed, the smart scouting approach allowed a less intense field campaign, since it allowed the use of satellite images to drive field activity, ensuring at the same time that the within-field variability is appropriately represented in the set of field measurements. Fig. 5c shows the relationship between mean LAI and PNC values (calculated on the data shown in the boxplots in Fig. 5a and b) and the LAI-derived Nc curves for cv. Selenio (solid line). Dashed lines indicate areas close to the Nc curve (NNI=1 ± 0.1), where nutritional status is assumed to be optimal (i.e., neither stress nor surplus) (Cilia et al., 2014). The colors of dots in Fig. 5c show how all the ESUs from Clusterc (red dots) were under limiting conditions (i.e., below the optimal condition area), whereas most of the Cluster-a ESUs (blue dots) belonged to non-limiting conditions areas (i.e., close to or above the Nc curve). ESUs sampled in Cluster-b (green dots) presented a more variable behavior, with severely stressed plants and others experiencing N luxury consumption. Overall, 10 ESUs out of 22 belonged to non-limiting conditions areas, whereas 12 to areas characterized by insufficient N availability. This analysis shows that field data taken with smart scouting approach and mobile devices reliably assessed the full range of values, confirming the effectiveness of both approaches.

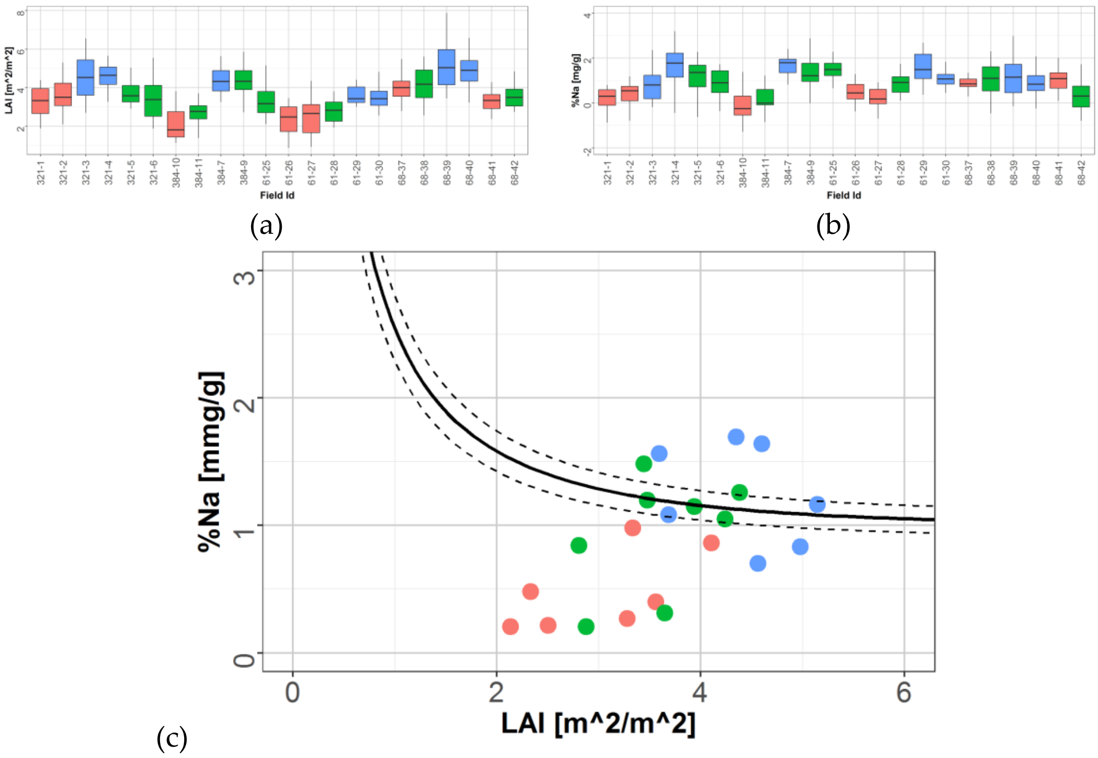

Figure 5. Boxplots of LAI (a) and PNC (b) values collected using the PocketLAI and PocketN smart apps for each ESU. Relative position of the 22 field data for the available ESUs is also shown with respect to the critical N curve (solid line). Dashed lines highlight area of "optimal status" around the dilution curve (i.e., NNI = 1±0.1) (c). Colours correspond to those used in Fig. 3 for ESU clustering.

3.2 Selection of regression models

ESUs and VIs from satellite images led to the regression coefficients shown in Table 4. In general, higher correlations were obtained for LAI data compared to PNC values. Many VIs showed correlation coefficients with LAI close to or above 0.7 with both sensors, whereas the best correlation with PNC barely reached values around 0.5. This was largely expected, since reflectance data are more influenced by plant tissue scattering (e.g., LAI and total biomass) rather than by leaf pigments. Moreover, it is well-known that chlorophylls and AGB are correlated for crops grown under non-artificially stressed conditions (Stroppiana et al., 2009). This is also the reason why—for radiative transfer approaches—the independent retrieval of LAI and chlorophyll content is an ill-posed problem, since different combinations of LAI and chlorophyll amount can cause the same spectral response (Combal et al., 2003). Fitzgerald et al. (2010), indeed, proposed to calculate a canopy chlorophyll content index (CCCI), which is considered a more robust variable. In any case, the regression coefficients reported here are comparable to those obtained in other similar studies by other authors (Chen et al., 2013; Huang et al., 2015; Zhao et al., 2015). Table 4 also shows that the accuracies obtained from RE images were slightly better than those achieved using the S2 sensor. Indeed, the LAI regression models achieved r2 higher than 0.7 for 11 VIs calculated from the RE image, but only for two VIs calculated from S2 data. The. difference between the two sensors was less pronounced for VI-PNC correlations, for which—despite the fact that the strongest correlation was achieved for an RE-based index (gNDVI, r2=0.56)—S2 data allowed deriving correlation coefficients consistent with RE ones for many VIs. The moderately better correlations obtained for RE VIs is likely due to the higher spatial resolution of this sensor (5 m, compared to 10m for S2) hence smaller area considered while extracting VI data. Moreover, some of the S2 bands used for VIs calculation, such as those corresponding to SWIR and REdg wavelengths, have even a coarser resolution (20 m) and the field campaign was conducted closer to RE's overpass date (see Table 2). It is interesting to notice that, for both sensors, the best correlations with LAI were obtained for VIs belonging to Vis-REdg (highest r2 MTVI2=0.77 for RE) and Vis-NIR (highest r2 MCARI=0.70 for S2) categories. Good correlations were also obtained with the single band of NIR from both sensors and with Vis-SWIR category from S2 images (not available for RE). Regarding PNC, satisfying results were usually obtained for Vis belonging to the Vis-NIR and Ratio category, with the best correlated VIs being gNDVI (r2=0.56) for RE and TCARI/OSAVI (r2=0.46) for S2. This is consistent with Haboudane et al. (2002), who observed that VIs in the Ratio category are more effective to estimate leaf biochemical features (like chlorophylls content) by minimizing the effect of plant structure. Good correlations were also achieved for both sensors using only the Red band; this region of the spectrum is indeed the one for which chlorophylls show the maximum absorption. Also Vis-REdg (NDVI2 and NDI45) and Vis-SWIR categories led to good results, although in this case only S2 images can be used, since the bands required for calculating those indices are not available in the RE sensor. In general, the analysis of regression coefficients for different VI categories revealed a good coherence among variables and sensors. Indeed, Vis that were well correlated to one of the field variables using one of the two sensors were also ranked first for the other. The VIs with the highest regression correlation (adjusted r2 value) were selected to define the empirical models for deriving LAI and PNC maps. In particular, MTVI2 and gNDVI were selected to spatialize LAI and PNC, respectively, for RE, whereas the corresponding S2 VIs were MCARI and TCARI/OSAVI. The regression models used to spatialize LAI and PNC data are showed in Fig. 6. It is important to underline that the selected VIs have an opposite behavior when correlated with the two field variables. In particular, MTVI2 and MCARI (selected for LAI) have a low correlation with PNC (maximum r2=0.27) and vice-versa for gNDVI and TCARI/OSAVI (maximum r2=0.58). This indirectly demonstrates their low autocorrelation. Despite the fact that other crops or EO products would most likely lead to other VIs being selected for estimating LAI and PNC, in many cases the best VIs would belong to the same category of those we selected. For instance, Cilia et al. (2014) identified MCARI/MTVI2 (Ratio category) as the most correlated with corn PNC on corn, and Xie et al. (2014) selected a Vis-NIR index to estimate LAI for winter wheat. Nevertheless, in other cases exactly the same VIs were selected to estimate LAI: Cilia et al. (2014) used MTVI2 whereas Huang et al. (2015) used MCARI. The same can be discussed for PNC: Quemada et al. (2014) used TCARI/OSAVI and Padilla et al. (2014) gNDVI. In general, also regression parameters retrieved by these authors are close to those showed in Fig. 6.

Table 4. Regression analyses between vegetation indices and field LAI and PNC data. Coefficient of determination (r^2) is reported. In bold, r^2 values higher than 0.60 for LAI and 0.40 for PNC are shown.

		LAI [m²/m²]		%PNC [mg/g]	
Category	Vegetation index	RapidEye	S2	RapidEye	S2
Vis	GLI	0.46	0.54	0.00	0.32
	Blue	0.25	0.24	0.35	0.28
	Green	0.01	0.05	0.31	0.22
	Red	0.47	0.47	**0.46**	**0.44**
Vis-RE	PSSR	/	0.56	/	0.24
	MCARI	**0.70**	**0.72**	0.12	0.22
	TCARI	**0.65**	0.32	0.29	0.34
	NDVI2	/	**0.62**	/	**0.44**
	NDI45	/	**0.66**	/	**0.41**
	MTCI	/	0.51	/	0.28
	S2REP	/	0.53	/	0.35
	IRECI	/	**0.61**	/	0.21
	TCI	**0.71**	**0.64**	0.29	0.36
Vis-RE-NIR	DCNI	0.01	0.41	0.15	0.35
Vis-RE-SWIR	MCARI$_{SWIR}$	/	**0.68**	/	0.33
	TCARI$_{SWIR}$	/	**0.67**	/	0.29
Vis-NIR	SR	**0.69**	0.57	0.26	0.25
	CI-G	0.54	0.53	**0.50**	0.35
	CVI	0.06	0.07	**0.45**	0.20
	MSAVI	**0.77**	**0.65**	0.22	0.25
	NDVI	**0.63**	**0.63**	0.39	**0.45**
	SAVI	**0.75**	**0.64**	0.23	0.27
	EVI	**0.73**	**0.65**	0.20	0.26
	gNDVI	0.58	0.56	**0.56**	**0.41**
	OSAVI	**0.73**	**0.65**	0.27	0.32
	MTVI2	**0.77**	**0.66**	0.23	0.27
Vis-SWIR	NRI	/	**0.65**	/	**0.43**
	NDFI	/	**0.66**	/	**0.43**
NIR-SWIR	OSAVI$_{SWIR}$	/	0.41	/	0.22
REd-NIR	CI-RE	**0.61**	0.54	0.37	0.30
	NDRE	**0.62**	0.58	**0.43**	0.38
REd	Red	0.11	0.02	0.03	0.15
NIR	NIR	**0.76**	**0.61**	0.18	0.20
Multiple Vis Ratio	MCARI/MTVI2	0.24	0.03	0.00	0.10
	NDRE/NDVI	0.57	0.55	**0.43**	0.36
	TCARI/SAVI	**0.71**	0.60	0.38	**0.46**
	TCARI/OSAVI	**0.70**	0.56	0.36	**0.46**
	TCARI/MSAVI	**0.71**	**0.61**	**0.41**	**0.45**
	TCARI/OSAVI$_{SWIR}$	/	0.53	/	0.23

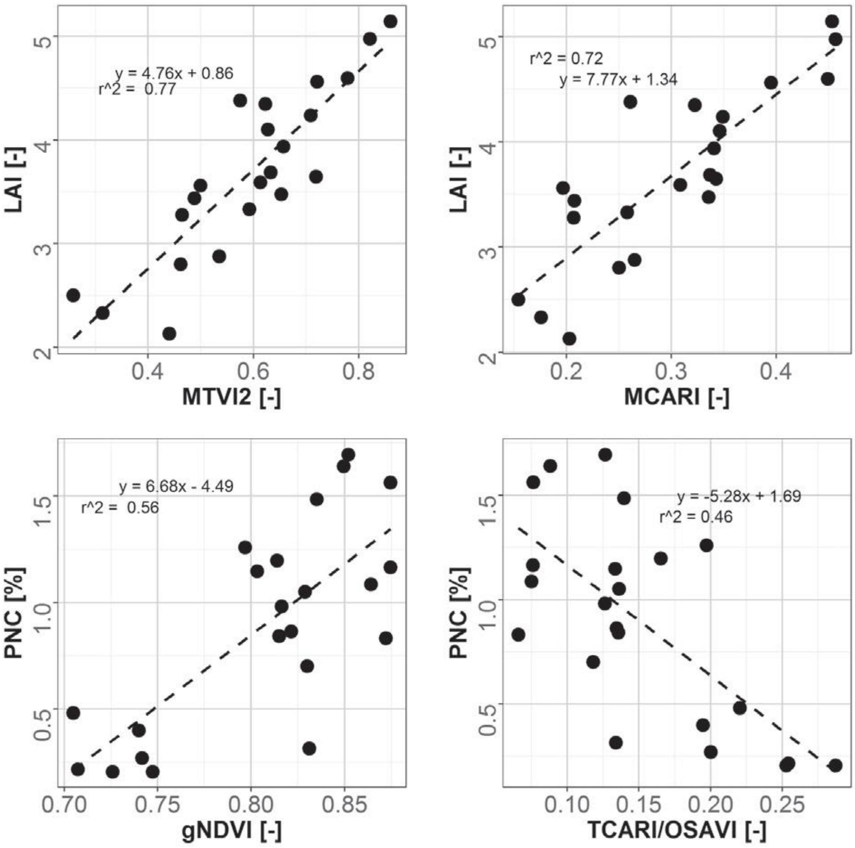

Figure 6. Selected linear regressions between field LAI and PNC data and selected VIs from RapidEye (RE) and Sentinel-2 (S2) sensors (left and right panels respectively).

3.3 Generation of NNI maps

Regression models (Fig. 6) allowed generating the NNI map shown in Fig. 7. Yellowish and greenish colors refer to areas in good nutritional status (NNI around 1) and luxury consumption (NNI > 1.1), respectively, whereas reddish indicates N deficiency (NNI < 0.9). NNI thresholds are based on Cilia et al. (2014). RE- and S2-based maps show the same spatial patterns of NNI in all fields. Indeed, the spatial correlation analysis performed between the two NNI maps showed a correlation coefficient of 0.72 (intercept=0.02, slope=0.97). Field #3 presented non-limiting conditions for N, whereas fields #1 and #2—despite the presence of some localized spots—were mainly characterized by insufficient N availability. Rice plants in field #4, instead, presented heterogeneous N nutritional status, with deficiencies shown in the top-corner and, to a lesser extent, in the right one. Observed spatial patterns have a clear agronomic interpretation. The luxury consumption in many areas of field #3 are explained by the use of the cover crop *Trifolium pretense* as green manure. The low NNI values calculated for a wide area in the top-right part of field #2 are due to sandy soil with low organic matter, which explain low-fertility soil regions within the field. Similar considerations can be done for the upper left corner of field #4, the soil presenting organic matter content lower than the rest of the paddy. Fig. 8 shows the NNI data as compared to the optimal value (NNI=1; black vertical line) and to the overall NNI mean (calculated on the pixels from all fields, NNI=0.78; red dotted vertical line). The high frequency of NNI values lower than 1 for fields #1 and #2 is even more clear, as well as the good nutritional status estimated for field #3.

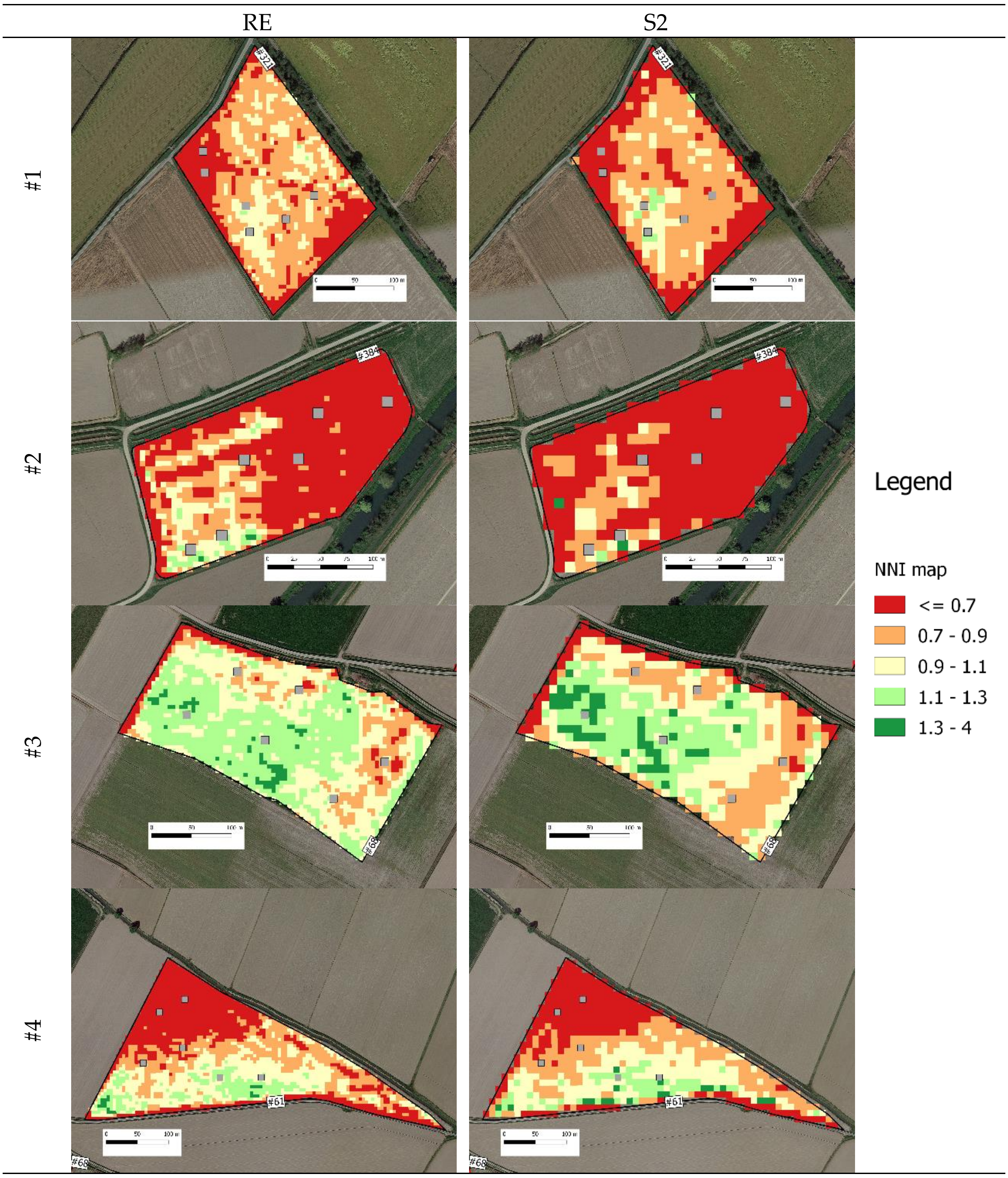

Figure 7. Nitrogen nutrition index (NNI) maps obtained from remotely sensed data of RapidEye (RE) and Sentinel-2 (S2). Optimal NNI value corresponds to 1. Grey squares indicate sampled elementary sampling units.

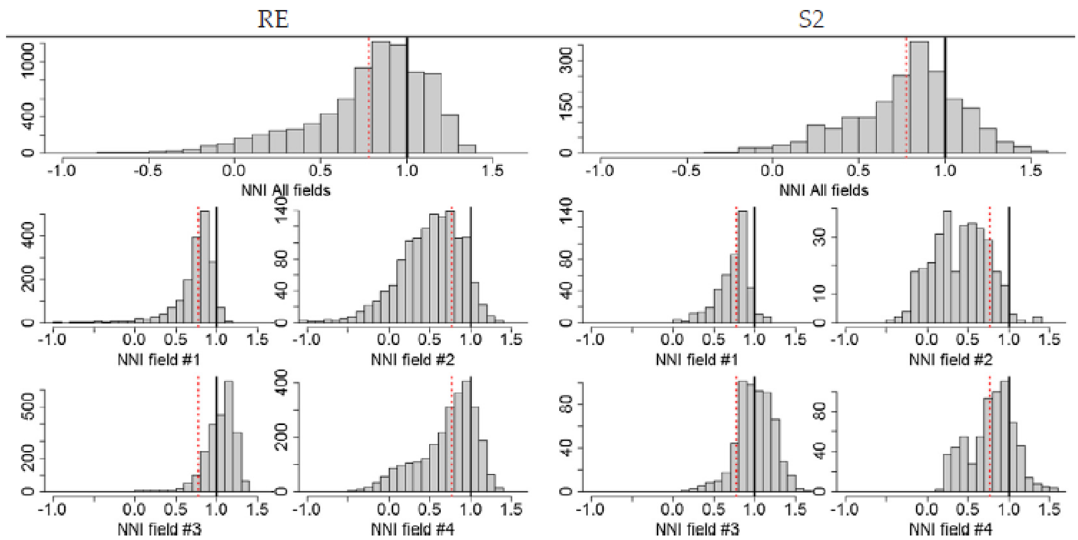

Figure 8. Values of nitrogen nutritional status (NNI) for all fields (top panel) and for each field separately (bottom panels) estimated using RapidEye (RE) and Sentinel-2 (S2) (left and right, panels respectively). Vertical black line and red dotted lines indicate NNI = 1 (optimum value) and general NNI mean, respectively.

3.4 Validation of NNI maps

Fig. 9 compares the values of NNI extracted from satellite-derived maps in correspondence of the ESUs with those calculated directly from field data (smart app measurements). The agreement between NNI values from satellite and ground measurements was slightly better when RE data were used (r2=0.54 vs. 0.47 for S2). Regression coefficients for both sensors are in line with what achieved by Chen et al. (2013) and Huang et al. (2015), who also worked on real farm conditions, with fields operationally managed by farmers rather than on plots with variability induced by experimental factors. Satellite-based NNI underestimated some of those derived from field data for NNI values above 1, and presented a slight overestimation for values close to zero, as already showed by Huang et al. (2015). These results can be considered as fully satisfactory, being in line with other studies although inexpensive and fast techniques were used to acquire field data (smart apps) and despite few ESUs were sampled in a single date. From the agronomic point of view, the worst case among those presented in Fig. 9 refers to the top-left area, since it represents an N stress not detected from satellite. On the other hand, the bottom-left area includes false positives, with luxury consumption detected from field data and stress conditions estimated from the satellite imagery. In any case, these two areas have the lowest density of points (Fig. 9). Indeed, N deficiencies were correctly identified in 18 out of 22 ESUs using RE data, and in 17 out of 22 cases using the S2 sensor. This kind of information on rice nutritional status, if timely supplied, could support farmers and agronomist in the tactical management of top-dressing fertilization. For instance, NNI maps can be used to drive further field scouting on more stressed areas, in order to allow farmers to thoroughly check the troublesome situations and, if needed, prioritize interventions. Additionally, NNI maps—together with expert based knowledge—can be used to develop prescription maps to perform top-dressing fertilizations by reducing the amount of N supplied in luxury consumption areas (NNI > 1.1) and increasing it in N-limited zones (NNI < 0.9) (Busetto et al., 2017). Alternatively, estimated NNI can be used in more quantitative ways, like in the operational services developed by Blondlot et al. (2005) and Chambenoit et al. (2004), or in the approaches tested under experimental conditions by Cilia et al. (2014) and Yang et al. (2014).

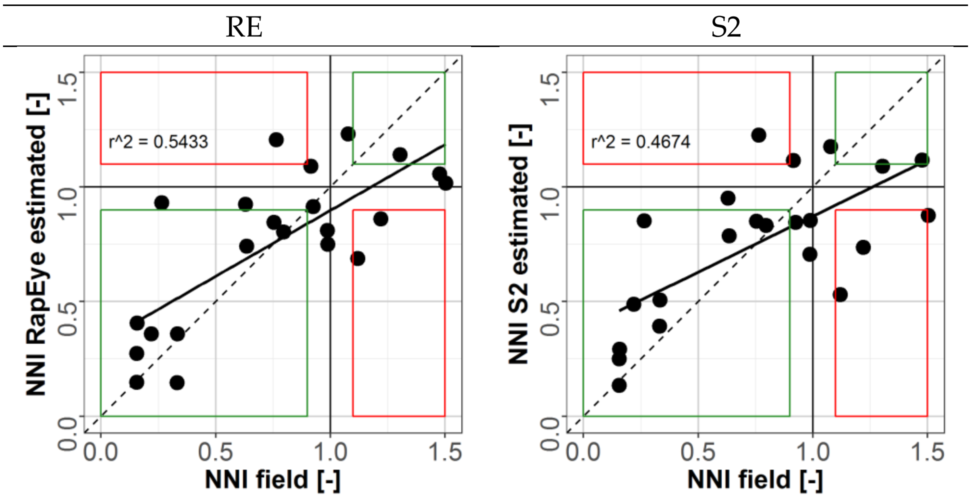

Figure 9. Relationship between values of nitrogen nutritional index (NNI) derived from satellites and estimated with ground measurements. Green and red boxes refer to good or poor coherence between the two series of NNI. The buffer of [0.9-1.1] represents the optimal nutritional condition. Grey dotted line indicates perfect agreement.

4 Conclusions

The need for increasing N use efficiency in rice-based cropping systems is justified by both its economic and environmental impact, since the amount of N not used by the plants does not enhance yield and unused nitrogen is at risk to have negative impact on water and air quality. This study demonstrated the feasibility—under real farming conditions—of a workflow for the production of NNI maps right after satellite image acquisition, using smart scouting techniques and smartphones as in-field sensors. The use of inexpensive and user friendly tools (like the PocketLAI and PocketN smart apps used here) for field activities have positive implications in terms of economic sustainability of the proposed methodology. Indeed, they extend the possibility to collect reliable data also to non-expert technicians. Moreover, smart scouting proved its time-effectiveness by prioritizing field data acquisition on few areas where the heterogeneity was maximum. NNI maps generated with the above-described method can be used to effectively monitor crops in near-real-time, and to highlight fields (or areas within a field) with severe N deficiency, hence prioritizing the fertilization activities and supporting the determination of applicable N amounts according to actual plant nutritional status. The spatial resolution of the maps developed in this study is suitable to perform variable rate fertilization, a key practice to increase N use efficiency. Moreover, our analysis demonstrated the feasibility of using satellite S2 products (operational and free-of-charge) to map rice nutritional status. Despite its lower resolution (ranging from 10m to 20 m) compared to that of the RE sensor (5 m), the resulting maps highlighted equivalent spatial patterns. The short revisit time of S2 (5 days when both A and B satellites of the constellation will be operational) fits farmer needs also in production districts where many varieties with different cycle lengths are sown in a 2-month time window and managed following different strategies in terms of number of events and N amount per event. These conditions determine a very heterogeneous spatial mosaic of crop conditions and actions to be performed to guarantee the sustainability of cropping systems. For these reasons, S2 (A and B) data seems to be the more suitable source of information for workflows like the one proposed in this paper. Furthermore, S2's spatial resolution (10 m) is consistent with the smallest area manageable with most VR machinery in areas like the Italian one, where double-disc spreaders are used, which are able to differentiate N amounts with a resolution of about 25 m. In practice, our analysis demonstrated the suitability of S2-like data in terms of both spatial and temporal resolution for monitoring N nutritional status and potentially for driving VR N distribution.

Acknowledgments

The research leading to these results was conducted within the ERMES FP7 project (http://www.ermes-fp7space.eu/) which received funding from the European Union Seventh Framework Program (FP7/ 2007-2013) under grant agreement 606983. This work was also supported by SATURNO project (https://www.progettosaturno.it/) funded by Regione Lombardia FEASR - PSR 2014-2020 program.

References

Agbu, P. a., Fehrenbacher, D.J., Jansen, I.J., 1990. Soil Property Relationships with SPOT Satellite Digital Data in East Central Illinois. Soil Science Society of America Journal 54, 807. doi:10.2136/sssaj1990.03615995005400030031x

Alam, M.M., Ladha, J.K., Khan, S.R., Foyjunessa, Harun-ur-Rashid, Khan, A.H., Buresh, R.J., 2005. Leaf color chart for managing nitrogen fertilizer in lowland rice in Bangladesh. Agronomy Journal 97, 949–959.

Ata-Ul-Karim, S.T., Yao, X., Liu, X., Cao, W., Zhu, Y., 2013. Development of critical nitrogen dilution curve of Japonica rice in Yangtze River Reaches. Field Crops Research 149, 149–158. doi:10.1016/j.fcr.2013.03.012

Ata-Ul-Karim, S.T., Zhu, Y., Yao, X., Cao, W., 2014. Determination of critical nitrogen dilution curve based on leaf area index in rice. Field Crops Research 167, 76–85. doi:10.1016/j.fcr.2014.07.010

Baret, F., de Solan, B., Lopez-Lozano, R., Ma, K., Weiss, M., 2010. GAI estimates of row crops from downward looking digital photos taken perpendicular to rows at 57.5° zenith angle: Theoretical considerations based on 3D architecture models and application to wheat crops. Agricultural and Forest Meteorology 150, 1393–1401. doi:10.1016/j.agrformet.2010.04.011

Basso, B., Dumont, B., Cammarano, D., Pezzuolo, A., Marinello, F., Sartori, L., 2016. Environmental and economic benefits of variable rate nitrogen fertilization in a nitrate vulnerable zone. Science of the Total Environment 545–546, 227–235. doi:10.1016/j.scitotenv.2015.12.104

Blackmore, S., 1994. Precision farming: an introduction. Outlook on Agriculture. doi:10.1177/003072709402300407

Blondlot, a, Gate, P., Poilvé, H., 2005. Providing operational nitrogen recommendations to farmers using satellite imagery. Precision Agriculture '05. Papers presented at the 5th European Conference on Precision Agriculture 123, 345–352.

Boschetti, M., Busetto, L., Manfron, G., Laborte, A., Asilo, S., Pazhanivelan, S., Nelson, A., 2017. PhenoRice: A method for automatic extraction of spatio-temporal information on rice crops using satellite data time series. Remote Sensing of Environment 194, 347–365. doi:10.1016/j.rse.2017.03.029

Boschetti, M., Stroppiana, D., Brivio, P. a., Bocchi, S., 2009. Multi-year monitoring of rice crop phenology through time series analysis of MODIS images. International Journal of Remote Sensing 30, 4643–4662. doi:10.1080/01431160802632249

Busetto, L., Casteleyn, S., Granell, C., Pepe, M., Barbieri, M., Campos-Taberner, M., Casa, R., Collivignarelli, F., Confalonieri, R., Crema, A., Garcia-Haro, F.J., Gatti, L., Gitas, I.Z., Gonzalez-Perez, A., Grau-Muedra, G., Guarneri, T., Holecz, F., Katsantonis, D., Minakou, C., Miralles, I., Movedi, E., Nutini, F., Pagani, V., Palombo, A., Paola, F. Di, Pascucci, S., Pignatti, S., Rampini, A., Ranghetti, L., Ricciardelli, E., Romano, F., Stavrakoudis, D.G., Stroppiana, D., Viggiano, M., Boschetti, M., 2017. Downstream Services for Rice Crop Monitoring in Europe: From Regional to Local Scale. IEEE Journal of Selected Topics in Applied Earth Observations and Remote Sensing. doi:10.1109/JSTARS.2017.2679159

Camera di Commercio Vercelli, 2013. Il bilancio economico dell'azienda risicola - Modello di impostazione ed esame di quattro casi rappresentativi.

Campos-Taberner, M., García-Haro, F.J., Camps-Valls, G., Grau-Muedra, G., Nutini, F., Busetto, L., Katsantonis, D., Stavrakoudis, D., Minakou, C., Gatti, L., Barbieri, M., Holecz, F., Stroppiana, D., Boschetti, M., 2017. Exploitation of SAR and optical sentinel data to detect rice crop and estimate seasonal dynamics of leaf area index. Remote Sensing 9, 1–17. doi:10.3390/rs9030248

Campos-Taberner, M., García-Haro, F.J., Camps-Valls, G., Grau-Muedra, G., Nutini, F., Crema, A., Boschetti, M., 2016. Multitemporal and multiresolution leaf area index retrieval for operational local rice crop monitoring. Remote Sensing of Environment 187, 102–118. doi:10.1016/j.rse.2016.10.009

Cao, Q., Miao, Y., Wang, H., Huang, S., Cheng, S., Khosla, R., Jiang, R., 2013. Non-destructive estimation of rice plant nitrogen status with Crop Circle multispectral active canopy sensor. Field Crops Research 154, 133–144. doi:10.1016/j.fcr.2013.08.005

Casa, R., Castrignanò, A., 2008. Analysis of spatial relationships between soil and crop variables in a durum wheat field using a multivariate geostatistical approach. European Journal of Agronomy 28, 331–342. doi:10.1016/j.eja.2007.10.001

Casa, R., Cavalieri, A., lo Cascio, B., 2011. Nitrogen fertilisation management in precision agriculture: A preliminary application example on maize. Italian Journal of Agronomy 6, 23–27. doi:10.4081/ija.2011.e5

Casa, R., Morari, F., 2016. La fertilizzazione di precisione, in: Edagricole (Ed.), Agricoltura Di Precisione. Bologna, pp. 249–272.

Casa, R., Pelosi, F., Pascucci, S., Fontana, F., Castaldi, F., Pignatti, S., Pepe, M., 2017. Early stage variable rate nitrogen fertilization of silage maize driven by multi-temporal clustering of archive satellite data, in: Advances in Animal Biosciences: Precision Agriculture (ECPA) 2017. pp. 288–292. doi:10.1017/S2040470017000103

Cerovic, Z.G., Masdoumier, G., Ghozlen, N.B., Latouche, G., 2012. A new optical leaf-clip meter for simultaneous nondestructive assessment of leaf chlorophyll and epidermal flavonoids. Physiologia Plantarum 146, 251–260.

Chambenoit, C., Laurent, F., Machet, J.M., Boizard, H., 2004. Development of a decision suport system for nitrogen management on potatoes, in: MacKerron, D.K.L., Haverkort, A.J. (Eds.), Decision Support Systems in Potato Production. Bringing Models to Practice. Wageningen Academic Publishers, Wageningen, the Netherlands, pp. 58–67. doi:10.3920/978-90-8686-527-7

Chen, P., 2015. A Comparison of Two Approaches for Estimating the Wheat Nitrogen Nutrition Index Using Remote Sensing. Remote Sensing 7, 4527–4548. doi:10.3390/rs70404527

Chen, P., Haboudane, D., Tremblay, N., Wang, J., Vigneault, P., Li, B., 2010. New spectral indicator assessing the efficiency of crop nitrogen treatment in corn and wheat. Remote Sensing of Environment 114, 1987–1997. doi:10.1016/j.rse.2010.04.006

Chen, P., Wang, J., Huang, W., Tremblay, N., Ou, Y., Zhang, Q., 2013. Critical nitrogen curve and remote detection of nitrogen nutrition index for corn in the northwestern plain of Shandong Province, China. IEEE Journal of Selected Topics in Applied Earth Observations and Remote Sensing 6, 682–689. doi:10.1109/JSTARS.2012.2236302

Cilia, C., Panigada, C., Rossini, M., Meroni, M., Busetto, L., Amaducci, S., Boschetti, M., Picchi, V., Colombo, R., 2014. Nitrogen status assessment for variable rate fertilization in maize through hyperspectral imagery. Remote Sensing 6, 6549–6565. doi:10.3390/rs6076549

Confalonieri, R., Debellini, C., Pirondini, M., Possenti, P., Bergamini, L., Barlassina, G., Bartoli, a., Agostoni, E.G., Appiani, M., Babazadeh, L., Bedin, E., Bignotti, a., Bouca, M., Bulgari, R., Cantore, a., Degradi, D., Facchinetti, D., Fiacchino, D., Frialdi, M., Galuppini, L., Gorrini, C., Gritti, a., Gritti, P., Lonati, S., Martinazzi, D., Messa, C., Minardi, a., Nascimbene, L., Oldani, D., Pasqualini, E., Perazzolo, F., Pirovano, L., Pozzi, L., Rocchetti, G., Rossi, S., Rota, L., Rubaga, N., Russo, G., Sala, J., Seregni, S., Sessa, F., Silvestri, S., Simoncelli, P., Soresi, D., Stemberger, C., Tagliabue, P., Tettamanti, K., Vinci, M., Vittadini, G., Zanimacchia, M., Zenato, O., Zetta, a., Bregaglio, S., Chiodini, M.E., Perego, a., Acutis, M., 2011. A new approach for determining rice critical nitrogen concentration. The Journal of Agricultural Science 149, 633–638. doi:10.1017/S0021859611000177

Confalonieri, R., Foi, M., Casa, R., Aquaro, S., Tona, E., Peterle, M., Boldini, a., De Carli, G., Ferrari, a., Finotto, G., Guarneri, T., Manzoni, V., Movedi, E., Nisoli, a., Paleari, L., Radici, I., Suardi, M., Veronesi, D., Bregaglio, S., Cappelli, G., Chiodini, M.E., Dominoni, P., Francone, C., Frasso, N., Stella, T., Acutis, M., 2013. Development of an app for estimating leaf area index using a smartphone. Trueness and precision determination and comparison with other indirect methods. Computers and Electronics in Agriculture 96, 67–74. doi:10.1016/j.compag.2013.04.019

Confalonieri, R., Gusberti, D., Bocchi, S., Acutis, M., 2006. The CropSyst model to simulate the N balance of rice for alternative management. Agronomy for Sustainable Development 26, 241–249. doi:10.1051/agro:2006022

Confalonieri, R., Paleari, L., Movedi, E., Pagani, V., Orlando, F., Foi, M., Barbieri, M., Pesenti, M., Cairati, O., La Sala, M.S., Besana, R., Minoli, S., Bellocchio, E., Croci, S., Mocchi, S., Lampugnani, F., Lubatti, A., Quarteroni, A., De Min, D., Signorelli, A., Ferri, A., Ruggeri, G., Locatelli, S., Bertoglio, M., Dominoni, P., Bocchi, S., Sacchi, G.A., Acutis, M., 2015. Improving in vivo plant nitrogen content estimates from digital images: Trueness and precision of a new approach as compared to other methods and commercial devices. Biosystems Engineering 135, 21–30. doi:10.1016/j.biosystemseng.2015.04.013

Fitzgerald, G., Rodriguez, D., O'Leary, G., 2010. Measuring and predicting canopy nitrogen nutrition in wheat using a spectral index-The canopy chlorophyll content index (CCCI). Field Crops Research 116, 318–324. doi:10.1016/j.fcr.2010.01.010

Fridgen, J.J., Kitchen, N.R., Sudduth, K.A., Drummond, S.T., Wiebold, W.J., Fraisse, C.W., 2004. Management Zone Analyst (MZA): Software for Subfield Management Zone Delineation. Agronomy Journal. doi:10.2134/agronj2004.1000

Grignani, C., Bassanino, M., Sacco, D., Zavattaro, L., 2003. Il bilancio degli elementi nutritivi per la redazione del piano di concimazione. Rivista di agronomia 37, 155–172.

Grisso, R., Alley, M., Holshouser, D., Thomason, W., 2009. Precision farming tools: soil electrical conductivity. Virginia Cooperative Extension 442, 1–6.

Guerif, M., Houles, V., Baret, F., 2007. Remote sensing and detection of nitrogen status in crops. Application to precise nitrogen fertilization. Progress of Information Technology in Agriculture 593–601.

Haboudane, D., Miller, J.R., Tremblay, N., Zarco-Tejada, P.J., Dextraze, L., 2002. Integrated narrow-band vegetation indices for prediction of crop chlorophyll content for application to precision agriculture. Remote Sensing of Environment 81, 416–426. doi:10.1016/S0034-4257(02)00018-4

Hansen, S., Jensen, H.E., Nielsen, N.E., Svendsen, H., 1991. Simulation of nitrogen dynamics and biomass production in winter wheat using the Danish simulation model DAISY. Fertilizer Research 27, 245–259. doi:10.1007/BF01051131

Holland, K.H., Schepers, J.S., 2010. Derivation of a variable rate nitrogen application model for in-season fertilization of corn. Agronomy Journal 102, 1415–1424. doi:10.2134/agronj2010.0015

Huang, S., Miao, Y., Zhao, G., Yuan, F., Ma, X., Tan, C., Yu, W., Gnyp, M., Lenz-Wiedemann, V., Rascher, U., Bareth, G., 2015. Satellite Remote Sensing-Based In-Season Diagnosis of Rice Nitrogen Status in Northeast China. Remote Sensing 7, 10646–10667. doi:10.3390/rs70810646

Jutz, S., Milagro-Pérez, M.P., 2017. Copernicus Program, in: Reference Module in Earth Systems and Environmental Sciences. doi:10.1016/B978-0-12-409548-9.10317-3

Karcher, D.E., Richardson, M.D., 2003. Quantifying turfgrass color using digital image analysis. Crop Science 43, 943–951.

Ke, J., Xing, X., Li, G., Ding, Y., Dou, F., Wang, S., Liu, Z., Tang, S., Ding, C., Chen, L., 2017. Effects of different controlled-release nitrogen fertilisers on ammonia volatilisation, nitrogen use efficiency and yield of blanket-seedling machine-transplanted rice. Field Crops Research 205, 147–156. doi:10.1016/j.fcr.2016.12.027

Kuenzer, C., Knauer, K., 2013. Remote sensing of rice crop areas. International Journal of Remote Sensing.

Lemaire, G., Jeuffroy, M.H., Gastal, F., 2008. Diagnosis tool for plant and crop N status in vegetative stage. Theory and practices for crop N management. European Journal of Agronomy 28, 614–624. doi:10.1016/j.eja.2008.01.005

Li, Y., Huang, L., Zhang, H., Wang, M., Liang, Z., 2017. Assessment of ammonia volatilization losses and nitrogen utilization during the rice growing season in alkaline salt-affected soils. Sustainability (Switzerland) 9. doi:10.3390/su9010132

Long, D.H., Lee, F.N., TeBeest, D.O., 2000. Effect of nitrogen fertilization on disease progress of rice blast on susceptible and resistant cultivars. Plant Disease 84, 403-409.

Longchamps, L., Khosla, R., 2015. Improving N use efficiency by integrating soil and crop properties for variable rate N management. Precision agriculture '15 249–256. doi:10.3920/978-90-8686-814-8_30

Mae, T., 1997. Physiological nitrogen efficiency in rice: Nitrogen utilization, photosynthesis, and yield potential. Plant and Soil 196, 201–210.

Munoz-Huerta, R.F., Guevara-Gonzalez, R.G., Contreras-Medina, L.M., Torres-Pacheco, I., Prado-Olivarez, J., Ocampo-Velazquez, R. V., 2013. A review of methods for sensing the nitrogen status in plants: advantages, disadvantages and recent advances. Sensors (Basel, Switzerland) 13, 10823–10843. doi:10.3390/s130810823

Navarro-Cerrillo, R.M., Trujillo, J., de la Orden, M.S., Hernández-Clemente, R., 2014. Hyperspectral and multispectral satellite sensors for mapping chlorophyll content in a Mediterranean Pinus sylvestris L. plantation. International Journal of Applied Earth Observation and Geoinformation 26, 88–96. doi:10.1016/j.jag.2013.06.001

NOMISMA, 2013. Import-export di riso: il ruolo dell'Italia nel contesto europeo. Rice imports and exports: Italy's role in the European context. Roma.

Onoyama, H., Ryu, C., Suguri, M., Iida, M., 2010. Estimation of Nitrogen Contents in Rice Plant at the Panicle Initiation Stage Using Ground-Based Hyperspectral Remote Sensing. IFAC Proceedings Volumes 43, 166–171. doi:10.3182/20101206-3-JP-3009.00029

Padilla, F.M., Pe, M.T., Gallardo, M., Thompson, R.B., 2014. Evaluation of optical sensor measurements of canopy reflectance and of leaf flavonols and chlorophyll contents to assess crop nitrogen status of muskmelon 58, 39–52. doi:10.1016/j.eja.2014.04.006

Pahlmann, I., Bottcher, U., Kage, H., 2017. Developing and testing an algorithm for site-specific N fertilization of winter oilseed rape. Computers and Electronics in Agriculture 136, 228–237. doi:10.1016/j.compag.2016.12.005

Peng, S., Garcia, F.V., Laza, R.C., Sanico, A.L., Visperas, R.M., Cassman, K.G., 1996. Increased N-use efficiency using a chlorophyll meter on high-yielding irrigated rice. Field Crops Research 47, 243–252.

Peng, S., Buresh, R.J., Huang, J., Yang, J., Zou, Y., Zhong, X., Wang, G., Zhang, F., 2006. Strategies for overcoming low agronomic nitrogen use efficiency in irrigated rice systems in China. Field Crops Research 96, 37–47. doi:10.1016/j.fcr.2005.05.004

Quemada, M., Gabriel, J.L., Zarco-Tejada, P., 2014. Airborne hyperspectral images and ground-level optical sensors as assessment tools for maize nitrogen fertilization. Remote Sensing 6, 2940–2962. doi:10.3390/rs6042940

Ranghetti, L., Busetto, L., Crema, A., Fasola, M., Cardarelli, E., Boschetti, M., 2016. Testing estimation of water surface in Italian rice district from MODIS satellite data. International Journal of Applied Earth Observation and Geoinformation 52, 284–295. doi:10.1016/j.jag.2016.06.018

Raun, W.R., Solie, J.B., Stone, M.L., Martin, K.L., Freeman, K.W., Mullen, R.W., Zhang, H., Schepers, J.S., Johnson, G. V., 2005. Optical Sensor-Based Algorithm for Crop Nitrogen Fertilization. Communications in Soil Science and Plant Analysis 36, 2759–2781. doi:10.1080/00103620500303988

Richter, R., Schlaepfer, D., 2016. Atmospheric/Topographic Correction for Satellite Imagery (ATCOR – 2/3 User Guide). Wessling, Germany. doi: 10.1017/ CBO9781107415324.004.

Salette, J., Lemaire, G., 1981. Sur la variation de la teneur en azote des graminées fourragères pendant leur croissance: Formulation d'une loi de diluition., Série III. ed. Compte Rendus de l'académie des Sciences, Paris.

Shimono, H., Okada, M., Yamakawa, Y., Nakamura, H., Kobayashi, K., Hasegawa, T., 2007. Lodging in rice can be alleviated by atmospheric CO_2 enrichment. Agriculture, Ecosystems & Environment 118, 223–230. doi:10.1016/j.agee.2006.05.015

Singh, U., Patil, S.K., Das, R.O., Padilla, J.L., Singh, V.P., Pal, A.R., 1999. Nitrogen dynamics and crop growth on an alfisol and a vertisol under rainfed lowland rice-based cropping system. Field Crops Research 61, 237–252. doi:10.1016/S0378-4290(98)00166-X

Stafford, J. V, Lark, R.M., Bolam, H.C., 1999. Using Yield Maps to Regionalize Fields into Potential Management Units, in: Precision Agriculture. pp. 225–237. doi:10.2134/1999.precisionagproc4.c20

Stroppiana, D., Boschetti, M., Brivio, P.A., Bocchi, S., 2009. Plant nitrogen concentration in paddy rice from field canopy hyperspectral radiometry. Field Crops Research 111, 119–129. doi:10.1016/j.fcr.2008.11.004

Stroppiana, D., Boschetti, M., Confalonieri, R., Bocchi, S., Brivio, P.A., 2006. Evaluation of LAI-2000 for leaf area index monitoring in paddy rice. Field Crops Research 99, 167–170. doi:10.1016/j.fcr.2006.04.002

Sukristiyonubowo, Kusumo, N., Muhrizal, S., 2012. Nitrogen, phosphorus and potassium removal by rice harvest product planted in newly opened wetland rice. International Research Journal of Plant Science 3, 63–68.

Varinderpal, S., Yadvinder, S., Bijay, S., Thind, H.S., Kumar, A., Vashistha, M., 2011. Calibrating the leaf colour chart for need based fertilizer nitrogen management in different maize (Zea mays L.) genotypes. Field Crops Research 120, 276–282. doi:10.1016/j.fcr.2010.10.014

Williams, J.R., Jones, C.A., Kiniry, J.R., Spanel, D.A., 1989. The EPIC Crop Growth Model. Transactions of the American Society of Agricultural Engineers1 32, 497–511. doi:10.13031/2013.31032

Xie, Q., Huang, W., Liang, D., Chen, P., Wu, C., Yang, G., Zhang, J., 2014. Indices Derived From Airborne Hyperspectral Images in Winter Wheat. Ieee Journal of Selected Topics in Applied Earth Observations and Remote Sensing 7, 3586–3594.

Xue, L., Yang, L., 2008. Recommendations for nitrogen fertiliser topdressing rates in rice using canopy reflectance spectra. Biosystems Engineering 100, 524–534. doi:10.1016/j.biosystemseng.2008.05.005

Yang, H., Yang, J., Lv, Y., He, J., 2014. SPAD Values and Nitrogen Nutrition Index for the Evaluation of Rice Nitrogen Status. Plant Production Science 17, 81–92. doi:10.1626/pps.17.81

Zhao, Q., Lenz-Wiedemann, V., Yuan, F., Jiang, R., Miao, Y., Zhang, F., Bareth, G., 2015. Investigating Within-Field Variability of Rice from High Resolution Satellite Imagery in Qixing Farm County, Northeast China. ISPRS International Journal of Geo-Information 4, 236–261. doi:10.3390/ijgi4010236